IN-45
0451/58

Semi-Annual Report on
Coupling Processes
between
Atmospheric Chemistry and Climate
NAS5-97039

Malcolm K. W. Ko, Debra K. Weisenstein, Run-Lie Shia,
Courtney J. Scott, and Nien Dak Sze

Atmospheric and Environmental Research

840 Memorial Dr.

Cambridge, MA 02139

Prepared for
NASA Atmospheric Chemistry Modeling and Data Analysis Program

March 18, 1999

Table of Contents

Abstract

This is the fourth semi-annual report for NAS5-97039, covering the time period July through December 1998. The overall objective of this project is to improve the understanding of coupling processes between atmospheric chemistry and climate. Model predictions of the future distributions of trace gases in the atmosphere constitute an important component of the input necessary for quantitative assessments of global change. We will concentrate on the changes in ozone and stratospheric sulfate aerosol, with emphasis on how ozone in the lower stratosphere would respond to natural or anthropogenic changes.

The key modeling tools for this work are the AER two-dimensional chemistry-transport model, the AER two-dimensional stratospheric sulfate model, and the AER three-wave interactive model with full chemistry. For this six month period, we report on a modeling study of new rate constant which modify the NO_x/NO_y ratio in the lower stratosphere; sensitivity to changes in stratospheric water vapor in the future atmosphere; a study of N_2O and CH_4 observations which has allowed us to adjust diffusion in the 2-D CTM in order to obtain appropriate polar vortex isolation; a study of SF_6 and age of air with comparisons of models and measurements; and a report on the Models and Measurements II effort.

(I) Evaluation of New Rates for NO_y Partitioning Reactions

Recent airborne measurements of NO and NO_y obtained during the POLARIS campaign, mostly at high northern latitudes in summer, indicate that the NO_x/NO_y partitioning calculated by models for the lower stratosphere is systematically underpredicted. Recent measurements of reaction rate constants which control NO_x/NO_y partitioning offer a possible resolution to the model/measurement disagreement. In conjunction with David Fahey's group at NOAA in Boulder who made the NO and NO_y measurements during the POLARIS campaign, we have performed model sensitivity studies to evaluate the effects of these rate revisions. A paper by Gao et al. (1999) has been submitted to Geophysical Research Letters detailing the measurements and model calculations of NO_x/NO_y ratio.

In the summer months at high latitudes, heterogeneous reactions do not play a large role in controlling the NO_x/NO_y ratio. Under these conditions, the ratio is largely controlled by the following reactions:

$$OH + NO \rightarrow HNO_3 + M \quad (R1)$$

$$OH + HNO_3 \rightarrow NO_3 + H_2O \quad (R2)$$

$$HNO_3 + h\nu \rightarrow OH + NO_2 \quad (R3)$$

The rates for reactions R1 and R2 reported in JPL-97 (DeMore et al., 1997) have recently been questioned. Donahue et al. (1997) first suggested that the rate for reaction R1 reported in JPL-97 may be too high. Dransfield et al. (1998) and Brown et al. (1998) reported new values for the rate of reaction R1 for stratospheric conditions which are about 20% lower than JPL-97 values. Brown et al. (1998) also reported values of the rate constant for R2 which are higher than the JPL-97 recommendation. Using a photochemical steady state box model, Gao et al. (1999) determined that agreement between models and measurements of NO_x/NO_y is much improved with the Brown et al. (1998) rates for R1 and R2 relative to the JPL-97 rates (model/measurement ratio increases from 0.62 to 0.84).

The Brown et al. (1998) rates for R1 and R2 have been incorporated into the AER 2-D chemical transport model. Figure 1a shows the change in calculated ozone for June of 2015 with subsonic aircraft included due to the modified rates relative to the JPL-97 rates. Ozone reductions of up to 5% are seen between 20 and 40 km altitude, while ozone increases are seen in the troposphere. Changes in ozone column (Figure 1b) exceed 1% only in northern polar regions. The percentage of ozone loss due to NO_x increases by 2-8% in the lower stratosphere, while that due to HO_x and ClO_x decreases. This change in the relative importance of the ozone loss cycles modifies the sensitivity of ozone to perturbations.

A new rate constant has also been measured for the reaction of NO_2 with O:

$$NO_2+O \rightarrow NO+O_2. \quad (R4)$$

This reaction does not affect the NO_x/NO_y partitioning significantly, but is a loss mechanism for odd oxygen. The new rate (A. R. Ravishankara, personal communication, 1998) is about 30% higher than the JPL-97 value at 200 K. Figure 2 shows the calculated changes in ozone due to inclusion of this modified reaction, along with R1 and R2, in the AER 2-D model. Local ozone is reduced by up to 13% at 30 km in the high latitudes, up to 6% at the equator at 30 km, and increased in the troposphere. Column ozone is reduced by 1-7% relative to a model with the JPL-97 rates.

We have calculated the ozone change due to HSCT emissions in 2015 (with 3.0 ppbv of Cl_y) and 2050 (with 2.0 ppbv of Cl_y) under two different emission scenarios. Both scenarios include 500 HSCTs operating at Mach 2.4 at 18-20 km altitude with an emission index (EI) for NO_x of 5, but scenario 1 includes no sulfur emissions, while scenario 2 includes sulfur emissions assuming $EI(SO_2)=0.4$ and 50%

conversion of the emitted sulfur to small particles in the aircraft wake. Table 1.1 summarizes the calculated annual average ozone column changes at 60°N. Without sulfur emissions, the Brown et al. rates for R1 and R2 lead to a slight increase in ozone depletion due to HSCT because of the increased importance of the NO_X cycle for ozone loss. With sulfur emissions, the new rates have the opposite effect. Ozone depletion due to emitted sulfur (which increases the stratospheric aerosol burden) is a function of the HO_X and ClO_X cycles, which are reduced under the new chemistry. Including new rates for reactions R1, R2, and R4 leads to even more ozone depletion due to HSCT for scenario 1 and even less ozone depletion for scenario 2. With R1, R2, and R4 updated, column ozone depletion at 60°N in 2015 is the same with or without sulfur emissions, and in 2050, column ozone depletion is greater without sulfur emissions than with sulfur emissions. We will be examining the the effect of modifications in R1, R2, and R4 on the sensitivity of ozone response to chlorine within the next few months.

Table 1: Annual average column ozone change at 60°N due to a fleet of 500 HSCTs operating at Mach 2.4 with EI(NO_X)=5 in the year 2015 or 2050.

HSCT	EI(SO_2)	with JPL-97 rates		R1, R2 updated		R1, R2, R4 updated	
Scenario		2015	2050	2015	2050	2015	2050
1	0	-0.5%	-0.5%	-0.6%	-0.6%	-0.8	-0.7
2	0.4	-1.3%	-0.9%	-1.0%	-0.5%	-0.8	-0.4

(II) Evaluation of Modified Stratospheric Water Vapor

For the 1998 NASA report on the impact of High Speed Civil Transport (HSCT) aircraft on the atmosphere, AER was asked to perform calculations with modified concentrations of stratospheric water vapor. Our standard treatment of H_2O fixes concentrations in the troposphere based on relative humidity and calculates H_2O in the stratosphere, using an imposed boundary condition at the tropopause. Stratospheric water vapor normally has mixing ratios of 3-6 ppmv. For these sensitivity studies, the tropopause boundary condition for H_2O was decreased by 2 ppmv, increased by 2 ppmv, and increased by 4 ppmv, resulting in commiserate changes in H_2O throughout the entire stratosphere. Increases in H_2O result in increases in HO_X, which increases ozone loss, particularly in the lower and upper stratosphere where HO_X forms the dominant ozone loss mechanism. Changes to background ozone concentrations under these three perturbations are shown in Figure 3 for a 2015 atmosphere with subsonic aircraft. Decreases of 2 ppmv in stratospheric H_2O result in increases in ozone column of 1-4%, with larger changes in polar springtime. Increases of 2 ppmv in stratospheric H_2O results in decreases in ozone column of 1-3%, with larger changes in polar springtime. Increases of 4 ppmv in stratospheric H_2O result in ozone column decreases of 2-7% outside the polar springtime regions, up to 12% in the northern polar spring and 15% in the southern polar spring. Local ozone changes in the upper stratosphere due to modified water are +12%, -8%, and -14% for H_2O decreases of 2 ppmv, increases of 2 ppmv, and increases of 4 ppmv, respectively. Changes in ozone in the mid-latitude lower stratosphere are as much as +8%, -8%, and -18% for H_2O decreases of 2 ppmv, increases of 2 ppmv, and increases of 4 ppmv, respectively.

The ozone response to HSCT is sensitivity to the background stratospheric water vapor concentration. At mid to high latitudes, especially in summer and fall, HO_X represents the dominant loss mechanism for ozone in the lower stratosphere. Decreases in H_2O (and HO_X) leads to an increase in the importance of the NO_X loss cycle in this region, resulting in a greater ozone response to HSCT. However, in the polar winter and spingtime, increases in H_2O concentration make the triggering of PSC

events by HSCT-emitted NO_x more likely. Figure 4 shows calculated changes in column ozone due to HSCT for the scenario with 500 HSCTs operating at Mach 2.4 with $EI(NO_x)=5$ and no sulfur emissions in 2015. For the case with H_2O reduced by 2 ppmv, maximum ozone depletion in the northern hemisphere occurs in late summer and fall; PSC events are not triggered. With the normal H_2O concentration, maximum depletion of 1.0% occurs in spring, but depletions of 0.6% are seen in summer also. With H_2O increased by 2 ppmv, summer ozone depletion is only -0.2%. With H_2O increased by 4 ppmv, springtime ozone depletion of up to 2% is calculated, and summertime shows incomplete recovery from the spring depletion. The sensitivity of ozone to increases in chlorine under these conditions of modified stratospheric water will be examined in the coming months.

(III) POLARIS Campaign and Analysis of 2-D CTM Transport

In conjunction with our participation in the POLARIS campaign, we have been analyzing the transport rates of the AER 2-D model and comparing modeled and derived quantities with available observations. Transport affects the ozone distribution directly by regulating the concentration of ozone and indirectly by influencing ozone production and loss through the concentrations of source and reservoir gases. Recent analyses using calculated SF_6 concentrations along with the derived mean age of air have been performed to test four different versions of transport within the AER 2-D CTM. Three of these have different horizontal mixing rates to simulate horizontal transport ranging from a weak tropical barrier to a strong tropical barrier. Recent analyses from the Models and Measurements II intercomparison exercise have indicated that many of the atmospheric models have circulations that are too vigorous (Hall et al. 1998). In response to this finding, one of the transport schemes scales the stream function by 0.6, creating slower velocities in both the horizontal and vertical directions. A comparative analysis of these models and *in situ* measurements was performed and general impacts on the HSCT assessment calculations were examined.

Using Geller et al.'s (1997) mean global tropospheric growth rate (equation 1) of SF_6 for the years 1987 through 1996, based on a wide range of tropospheric measurements,

$$[SF_6](t) = 3.4361 + 0.2376(t - 1996) + 0.0049(t - 1996)^2 \quad (1)$$

and Volk et al.'s (1997) derived equation which directly relates the SF_6 (pptv) concentration to a mean age of air (equation 2),

$$[SF_6](x,t) = [SF_6](t-\Gamma-\delta\Gamma) + 2c\Lambda(\Gamma-\delta\Gamma). \quad (2)$$

SF_6 concentrations and the mean age of air for the four different transport versions were calculated. Here, $[SF_6](x,t)$ is the SF_6 concentration in pptv at point (x,t) in space and time, $\delta\Gamma$ is the tropospheric lag time (0.8 years), Γ is defined as the mean age of air in years (first moment of the Green's function), c is 0.0049 pptv/yr^2 and Λ (1.25 years) parameterizes an appropriate value of the width of the age spectrum by using a weighted average of two GCM outputs. Measurements of SF_6 and N_2O concentration were used from the Stratospheric Tracers of Atmospheric Transport (STRAT) (Elkins, et al., 1996), the Airborne Southern Hemisphere Ozone Experiment/Measurements for Assessing the Effects of Stratospheric Aircraft (ASHOE/MAESA) (Tuck, et al. 1997), and the Photochemistry of Ozone Loss in the Arctic Region In Summer (POLARIS) campaigns to compare the different transport versions of the model.

Figure 5 shows the calculated 1996 annual average age of air in years as a function of the annual average N_2O concentration (ppbv) for each of the versions of the AER 2-D CTM with the *in situ* measurements overlaid. Three regions of the models are represented: the southern mid-latitudes, the tropics and the northern mid-latitudes. In all versions of the model, the northern mid-latitude region calculates the oldest ages of air. The youngest ages of air are seen in the tropical region. This is directly attributed to the large scale transport, with a weaker hemispheric motion moving the SF_6 concentrations into the northern hemisphere and large scale flow from the troposphere entering the stratosphere via the tropical tropopause.

Figure 6 illustrates the annual average 1996 calculated mean age of air as a function of latitude and N_2O concentration with the *in situ* measurements overlaid. Younger air is seen at high tropical altitudes in the LEAKY-PIPE (panel b) and the PIPE (panel c) versions of the model, indicative of a stronger tropical upwelling in these versions of the model. The LEAKY-PIPE and PIPE show similar structure in the age contours, with the PIPE version calculating the youngest ages overall. The NO-PIPE (panel a) and the SLOW (panel d) versions of the model resemble one another qualitatively but the SLOW model calculates ages of air that are much older than the NO-PIPE version. The SLOW transport version (panel d) closely resembles the measurements, both qualitatively and quantitatively, calculating the flattest contours in the lower altitudes and the oldest ages of air in the higher latitudes and altitudes

Figure 7 shows the change in calculated column ozone as a function of latitude and season for a 500 aircraft fleet with emission index of 5, flying in a 2015 atmosphere, with background aerosols. Inspection of Figure 7 shows the largest ozone depletion due to the HSCT perturbation, in the SLOW (panel d) version of the model. Total column ozone change in the SLOW version of the model for the northern mid-latitudes ranges from –0.5% to -0.8% loss in contrast to the value of ~-0.3% in the NO-PIPE (panel a) version of the model. The larger ozone loss in the NH is directly due to the change in the transport quantities, where a stronger barrier coupled with a slower stream function prevents much of the aircraft exhaust to circumvent the globe. The LEAKY-PIPE, and PIPE ozone responses, shown in panels b and c respectively, fall between the SLOW and NO-PIPE responses.

Although the SLOW version of the model gives reasonable agreement with the *in situ* measurements of SF_6 concentration, its calculated ages, and various other tracer species, it is not necessarily a consistently better transport scheme in all regions of the atmosphere. Table 2 shows calculated global lifetimes in years for selected tracers from all versions of the AER 2-D model. Also shown in Table 2 are calculated ages, based on *in situ* measurements, from Volk et al. (1997) Comparison of the global ages derived from *in situ* measurements with the four different transport versions of our model give clues to transport issues. All of the versions of the model give different ages, with the PIPE giving the youngest and the SLOW giving the oldest ages. Notably, the SLOW version calculates ages that are erroneously long for all species not dependent on OH chemistry.

Based on Figure 5, which shows age of air vs N_2O for the four versions of the AER 2-D CTM, the question arises why the SLOW model does not match Volk's calculated lifetime for N_2O. Careful analysis indicates that the age of air, in the AER model, does not share the same mixing surfaces with other long-lived species. This does not indicate to what extent the real atmosphere is in steady state and whether true SF_6 concentrations share the mixing surfaces of other long-lived species in the atmosphere. It does however, merit careful consideration when trying to extrapolate theory to the real atmosphere.

Table 2: Calculated global lifetimes (years) for selected species from the AER 2-D models. Lifetimes calculated by Volk et al. (1997), based on correlations with age of air, are included for comparison.

SPECIES	SLOW	NO-PIPE	LEAKY-PIPE	PIPE	VOLK et al.
N_2O	171.0	131.2	112.3	102.1	124 +/- 49
$C_2Cl_3F_3$	122.1	94.2	78.7	71.8	89 +/- 35
$CBrClF_2$	52.2	38.1	33.8	32.3	20 +/- 9
$CFCl_3$	74.0	56.4	48.4	45.3	41 +/- 12
CF_2Cl_2	147.1	112.4	95.0	85.8	77 +/- 26
CCl_4	63.0	48.0	41.6	39.3	32 +/- 11
CH_3CCl_3	7.0	6.1	6.0	5.8	-
CH_4	12.7	11.3	11.2	11.0	-

(IV) Model Adjustment of Mixing Rates across the Polar Barriers

The results of the Models and Measurements II experiments showed that there are significant defects in the transport parameters currently used in most 2-D chemistry transport models. One of these defects is the lack of a clear polar vortex. Large amounts of observations and measurements show that the fast isentropic mixing created by the planetary wave breaking cannot penetrate into the polar vortex and the concentrations of long-lived species, e.g. N_2O and CH_4, have strong gradients rapidly across the polar vortex well. This feature is not seen in the results of the AER 2-D CTM (Figure 8a). The isentropic mixing is represented by the eddy diffusion coefficient, K_{yy} in the 2-D CTM. Smaller values of K_{yy} should be assigned in the polar barrier to simulate the polar vortex. The measurements of long-lived species by instruments aboard of UARS with nearly global coverage and high precision provide a useful database for adjusting K_{yy} across the polar vortex. Recently, Randel et al. (1998) processed the UARS/MLS and UARS/CLAES CH_4 data to create the altitude-equivalent latitude distributions of CH_4 by averaging the data along the potential vorticity (PV) contours to avoid smoothing the gradients of CH_4 distribution across the vortex edge. These new 2-D distributions of CH_4 reveal the polar barriers, which greatly reduce the mixing between the mid-latitudes and polar region (Figure 8b).

During the past 6 months, we have used these CH_4 distributions to adjust the mixing across the polar vortex in the AER 2-D CTM. We define a cost function to measure the difference between the gradients of the CH_4 on the polar vortex edge from the model simulations and from Randel's data. By adjusting the K_{yy} to minimizing the cost function calculated using a 2-D CTM model with parameterized CH_4 chemistry, we derive values for K_{yy} near the polar vortex. The values of K_{yy}, which produce the minimum for the cost function have significantly improved the model simulations of CH_4 across the polar barrier (Figure 8c). These adjusted values of K_{yy} for both north and south polar vortices were used in the 2-D CTM with detailed photochemistry. The new version of the full 2-D model improves the simulations of other long-lived species in the polar region. Unlike in the subtropical barrier case, the adjustment of K_{yy} in the polar barrier only has localized effects on the age of air calculation and the simulated atmospheric effects of the High Speed Civil Transport (HSCT). The exchange time scale between the polar vortex and the middle latitudes is calculated using the same method as for the subtropical barrier (Shia et al, 1998). This study was presented at the 1998 AGU Fall Meeting and is reproduced here as Appendix B.

(V) Activity Associated with the Models and Measurements Workshop II

After the March 1998 meeting, drafts of different sections were collected from various authors. Malcolm Ko, Charles Jackman, Alan Plumb and Karen Sage met at NASA GSFC on October 6 for a one day meeting to finalize the structure of the report. The draft report was sent to NASA Langley in December for copy editing.

(VI) Publications Supported by this Contract

Papers that have appeared or are in press

(1) Shia R.-L., M. K. W. Ko, D. K. Weisenstein, C. Scott and J. Rodriguez, Transport between the tropical and mid-latitude lower stratosphere: Implications for ozone response to high-speed civil transport emissions, *J. Geophys. Res., 103,* 25,435-25,446, 1998.

(2) Ko, M. K. W., N. D. Sze, C. Scott, J. M. Rodriguez, D. K. Weisenstein, and S. P. Sander, Ozone depletion potential of CH_3Br, *J. Geophys. Res., 103,* 28,187-28,195, 1998.

(3) Danilin, M. Y., J. M. Rodriguez, W. Hu, M. K. W. Ko, D. K. Weisenstein, J. B. Kumer, J. L. Mergenthaler, J. M. Russell III, M. Koike, and G. K. Yue, Nitrogen species in the post-Pinatubo stratosphere: Model analysis utilizing UARS measurements, *J. Geophys. Res.*, in press, 1999.

Papers that have been submitted

(4) Gao, R. S., D. W. Fahey, L. A. Del Negro, S. G. Donnelly, E. R. Keim, L. Teverovski, P. O. Wennberg, T. F. Hanisco, M. H. Proffitt, J. J. Margitan, J. C. Wilson, J. W. Elkins, R. M. Stimpfle, R. C. Cohen, C. T. McElroy, T. P. Bui, R. J. Salawitch, S. S. Brown, A. R. Ravishankara, R. W. Portmann, M. K. W. Ko, D. K. Weisenstein, and P. A. Newman, A comparison of observations and model simulations of NO_X/NOy in the lower stratosphere, submitted to *Geophys. Res. Lett.*, 1999.

(5) Danilin, M. Y., M. L. Santee, J. M. Rodriguez, M. K. W. Ko, J. M. Mergenthaler, J. B. Kumer, and A. Tabazadeh, Trajectory hunting: Analysis of UARS measurements showing rapid chlorine activation, submitted to *J. Geophys. Res.,* 1999.

(6) Tabazadeh, A., M. L. Santee, H. C. Pumphrey, P. A. Newman, M. Y. Danilin, J. L. Mergenthaler, P. Hamill, and N. Livesey, Arctic ozone hole in a denitrified future colder stratosphere, submitted to *Nature*, 1999.

(VII) References Cited

Brown, S. S., et al., Role of nitrogen oxides in the lower stratosphere: A reevaluation based on laboratory studies, submitted to *Geophys. Res. Lett.*, 1998.

DeMore, W. B., et al., Chemical kinetics and photochemical data for use in stratospheric modeling, *JPL Publ. 97-4,* Jet Propulsion Lab, Pasadena, CA, 1997.

Donahue, N. M., M. Dubey, R. Mohrschladt, K. L. Demerjian, and J. G. Anderson, A high pressure flow study of the reactions of $OH+NO_X$-->$HONO_X$: Errors in the falloff region, *J. Geophys. Res., 102,* 6159-6168, 1997.

Dransfield, T. J., K. K. Perkins, N. M. Donahue, J. G. Anderson, M. M. Sprengnether, and K. L. Demerjian, Temperature and pressure dependent kinetics of the gas-phase reaction of the hydroxyl radical with nitrogen dioxide, *Geophys. Res. Lett., 26,* 687-690, 1999.

Elkins, J.W., D.W. Fahey, J.M. Gilligan, G.S. Dutton, T.J. Baring, C.M. Volk, R.E. Dunn R.C. Myers, S. A. Montzka, P.R. Wamsley, A.H. Hayden, J.H. Butler, T. M. Thompson, T. H. Swanson, E.J. Dlugokencky, P.C. Novelli, D. F. Hurst, J. M. Lobert, S.J. Ciciora, R. J. McLaughlin, T. L. Thompson, R. H. Winkler, P. J. Fraser, L. P. Steele, M. P. Lucarelli, Airborne gas chromatograph for in situ measurements of long lived species in the upper troposphere and lower stratosphere, *Geophys. Res. Lett.., 23,* 347-350, 1996.

Gao, R. S., D. W. Fahey, L. A. Del Negro, S. G. Donnelly, E. R. Keim, L. Teverovski, P. O. Wennberg, T. F. Hanisco, M. H. Proffitt, J. J. Margitan, J. C. Wilson, J. W. Elkins, R. M. Stimpfle, R. C. Cohen, C. T. McElroy, T. P. Bui, R. J. Salawitch, S. S. Brown, A. R. Ravishankara, R. W. Portmann, M. K. W. Ko, D. K. Weisenstein, and P. A. Newman, A comparison of observations and model simulations of NO_X/NOy in the lower stratosphere, submitted to *Geophys. Res. Lett.*, 1999.

Geller L.S., J.W. Elkins, J.M. Lobert, A.D. Clarke, D.F. Hurst, J.H. Butler, and R.C. Myers, Tropospheric SF_6: Observed latitudinal distribution and trends, derived emissions and interhemispheric exchange time, Geophys. Res. Lett.., 24, 675-678, 1997.

Hall, T.M., and R.A. Plumb, Age as a diagnostic of stratospheric transport, *Geophys. Res. Lett., 99,* 1059-1070, 1994.

Hall, T. M., D. W. Waugh, K. A. Boering, and R. A. Plumb, Evaluation of transport in stratospheric models, *J. Geophys. Res.*, in press, 1999.

Randel, W. J., F. Wu, J. M. Russell III, A. Roche, and J. W. Waters, Seasonal cycle and QBO variations in stratospheric CH_4 and H_2O observed in UARS HALOE Data, *J. Atoms. Sci., 55,* 163-185, 1998.

Shia R.-L., M. K. W. Ko, D. K. Weisenstein, C. Scott and J. Rodriguez, Transport between the tropical and mid-latitude lower stratosphere: Implications for ozone response to high-speed civil transport emissions, *J. Geophys. Res., 103,* 25,435-25,446, 1998.

Volk, C.M., J. W. Elkins, D.W. Fahey, G. S. Dutton, J. M. Gilligan, M. Loewenstein, J. R. Podolske, and K. R. Chan, On the evaluation of source gas lifetimes from stratospheric observations, *J. Geophys. Res., 102,* 25543-25564, 1997.

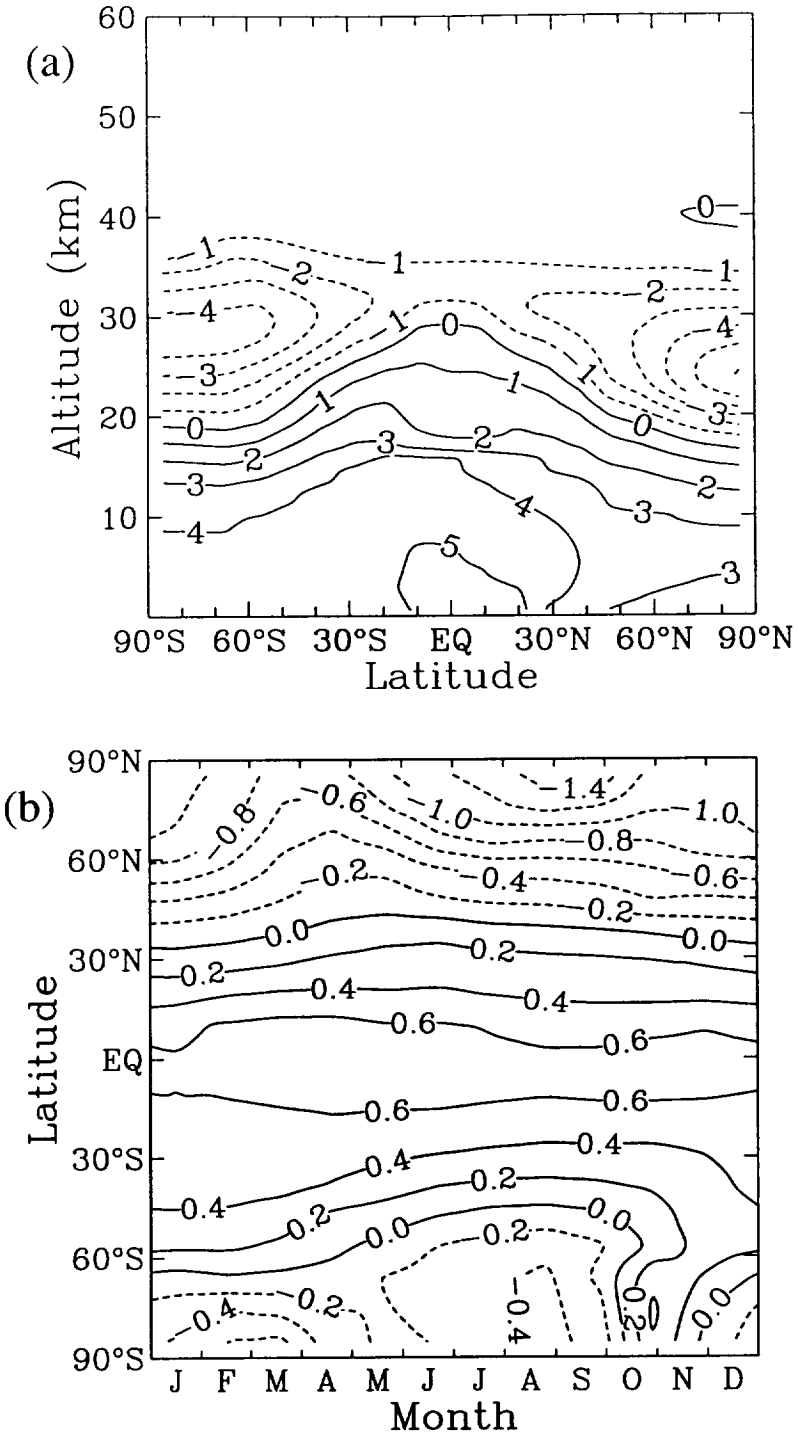

Figure 1: Calculated percentage change in (a) local ozone in June, and (b) total column ozone due to modifying the rates for reactions R1 and R2 from JPL-97 values to those reported by Brown et al. (1998). Results shown are for 2015 with subsonic aircraft emission included.

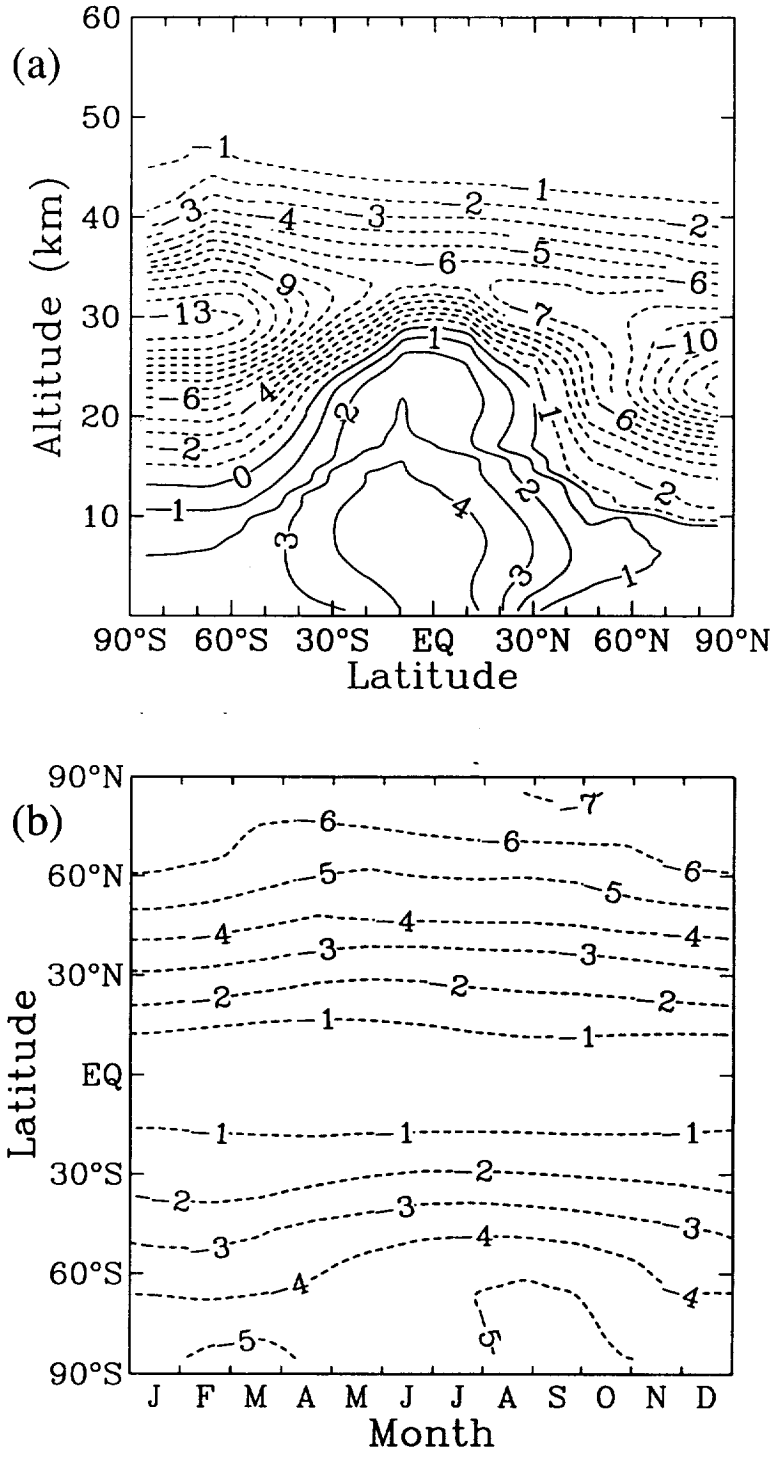

Figure 2: Calculated percentage change in (a) local ozone in June, and (b) total column ozone due to modifying the rates for reactions R1, R2, and R4 from JPL-97 values to those reported by Brown et al. (1998) and Ravishankara (personal communication, 1998). Results shown are for 2015 with subsonic aircraft emission included.

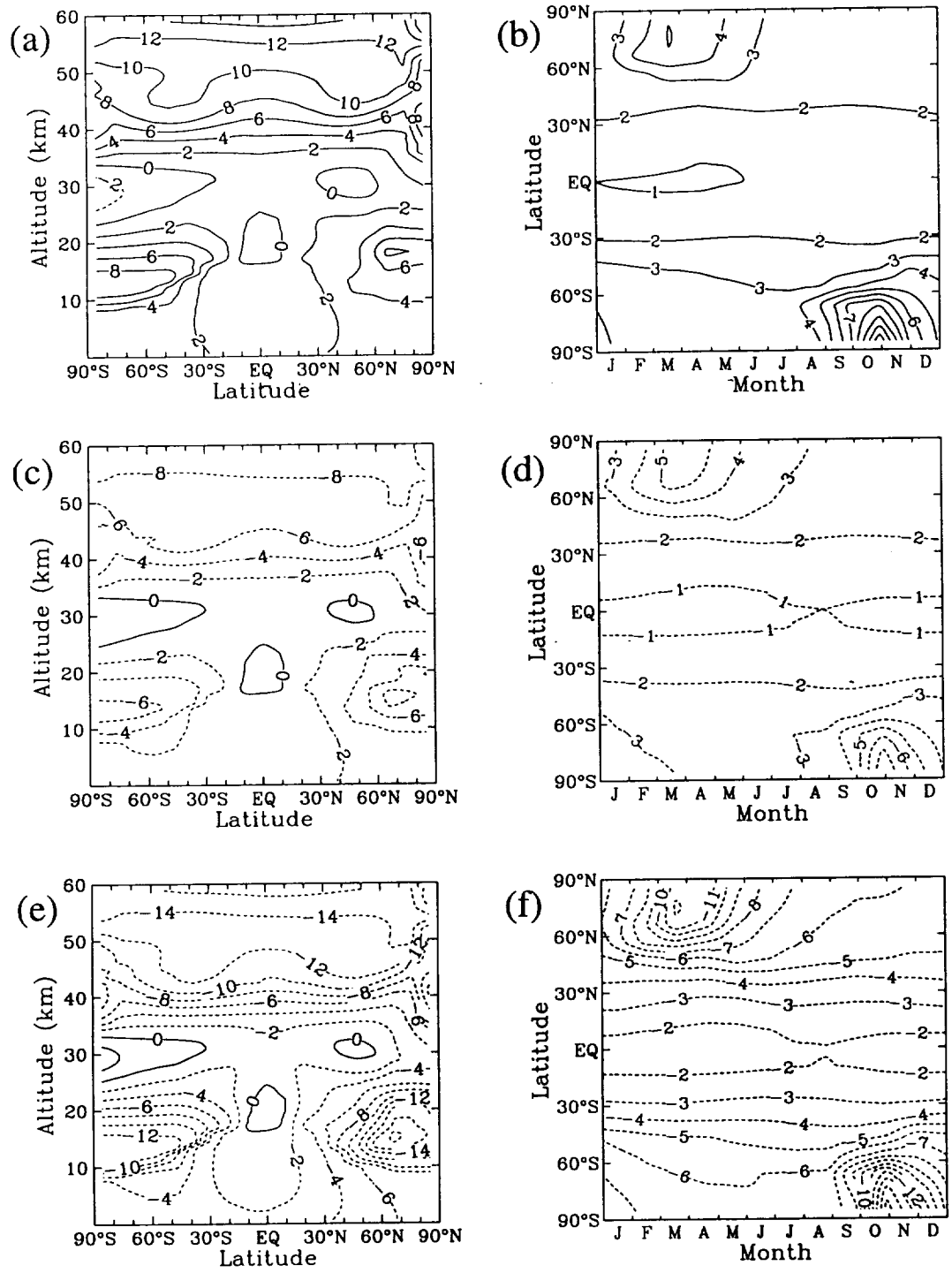

Figure 3: Calculated changes in June ozone (left column) and total ozone (right column) due to changes in stratospheric H_2O relative to the standard treatment in the AER 2-D model. Panels (a) and (b) have stratospheric H_2O reduced by 2 ppmv, panels (c) and (d) have stratospheric H_2O increased by 2 ppmv, and panels (e) and (f) have stratospheric H_2O increased by 4 ppmv. All calculations represent the 2015 atmosphere with a subsonic aircraft fleet.

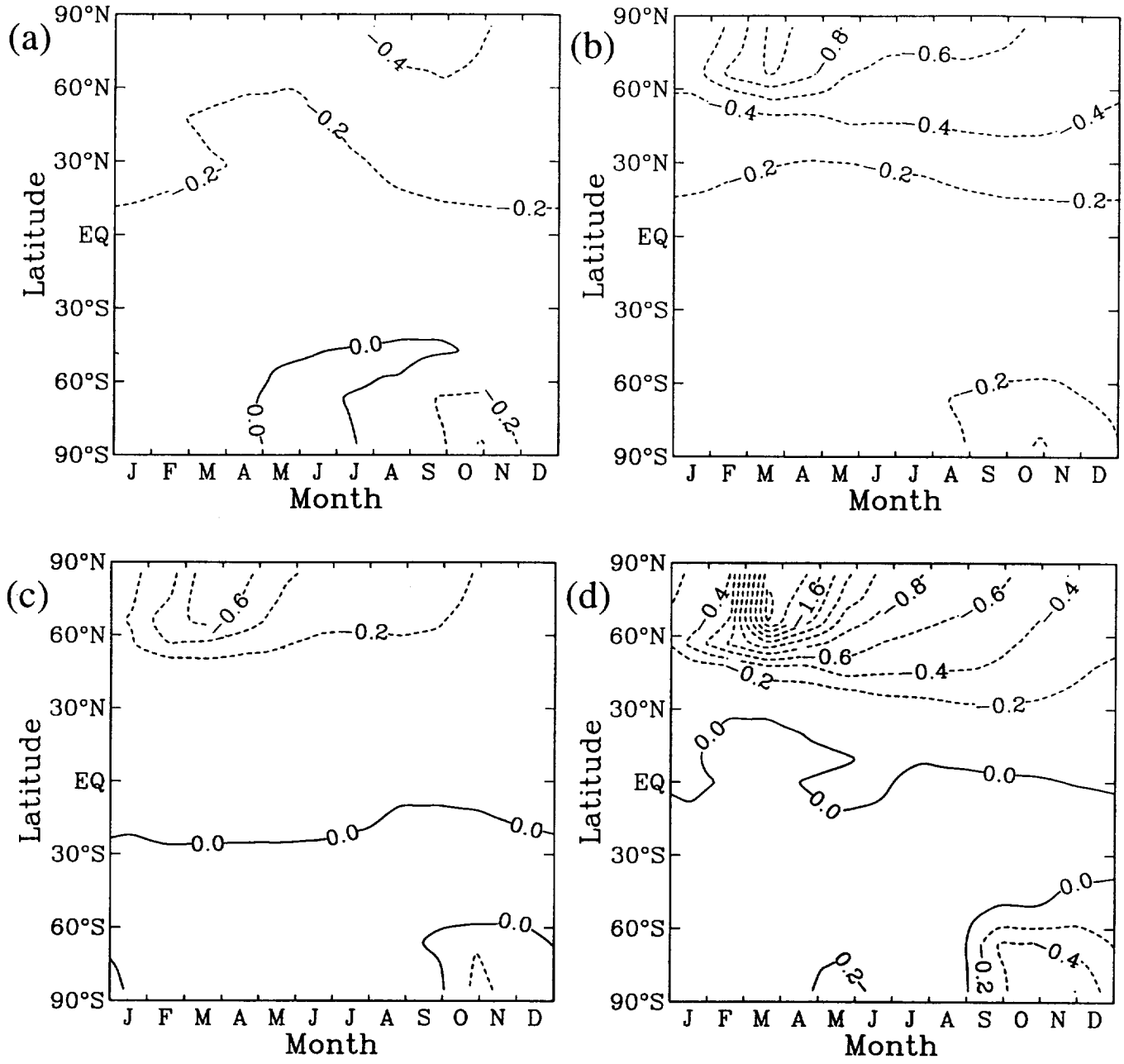

Figure 4: Calculated changes in total column ozone due to an HSCT fleet of 500 aircraft operating at Mach 2.4 with EI(NO_x)=5 in 2015 with nonvolcanic aerosol surface area SA0. Panel (a) is with stratospheric H_2O decreased by 2 ppmv, panel (b) with stratospheric H_2O at normal levels, panel (c) with stratospheric H_2O increased by 2 ppmv, and panel (d) with stratospheric H_2O increased by 4 ppmv.

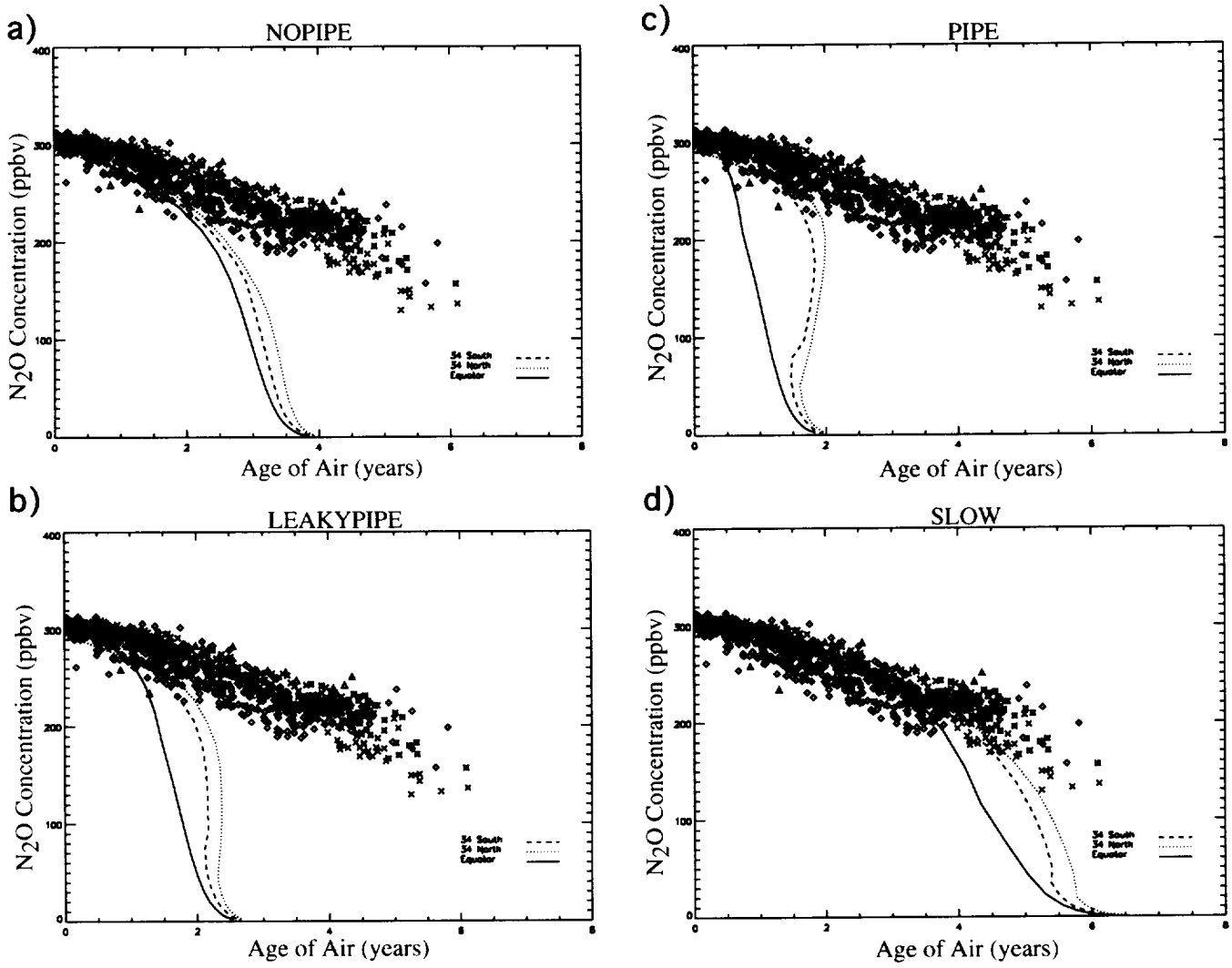

Figure 5: Calculated 1996 annual average age of air in years for all latitudes and altitudes as a function of N_2O concentration (ppbv). Insitu measurements are represented by symbols. Profiles from 35°N, the Equator and 35°S are represented with various line styles. The NO-PIPE version is displayed in panel (a), the LEAKY-PIPE version in panel (b), the PIPE in panel (c) and the SLOW in panel (d).

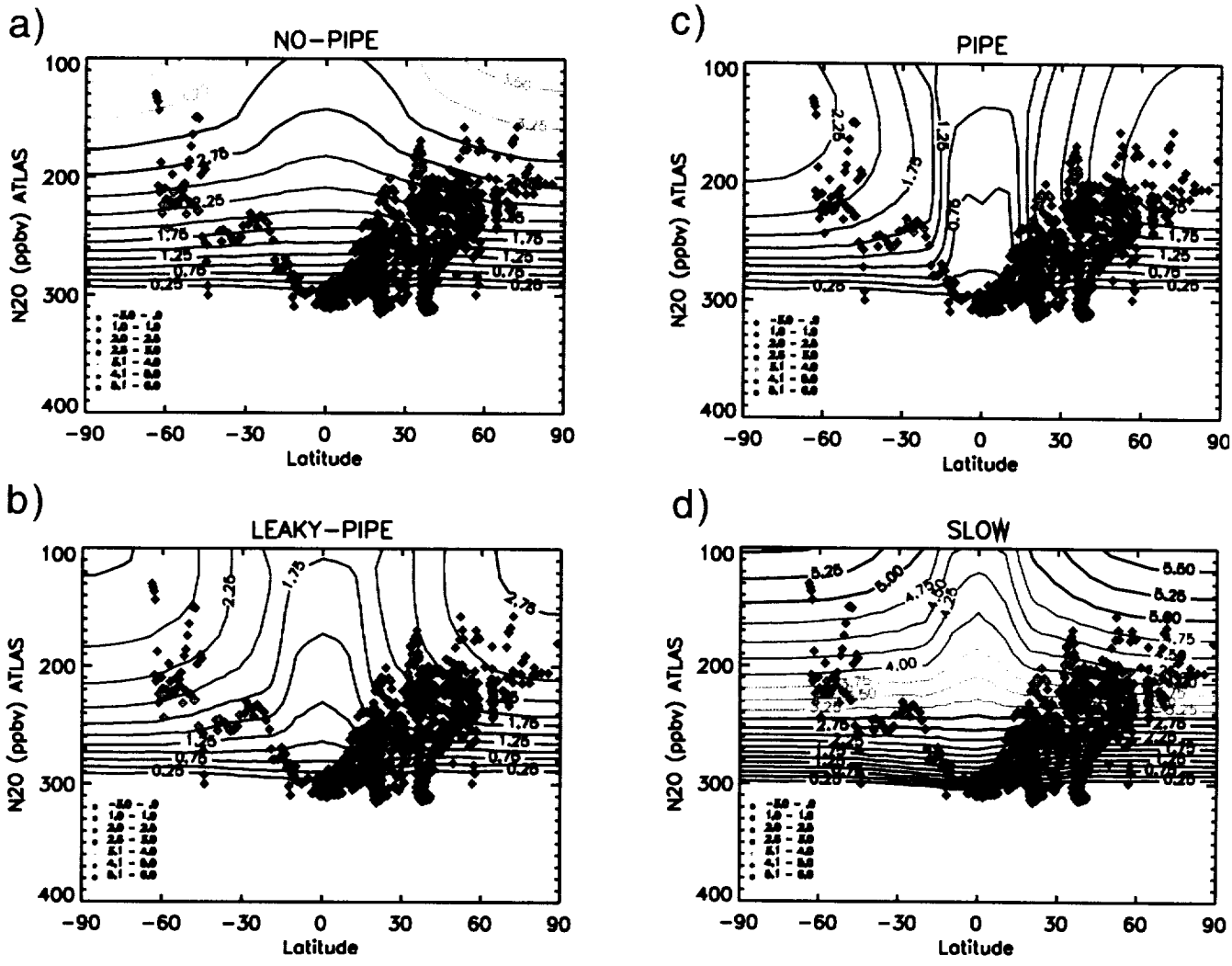

Figure 6: Annually averaged 1996 calculated age of air (years) from SF_6 concentrations for the four AER 2-D CTMs as a function of latitude and N_2O. Filled circles represent the corresponding *in situ* measurements. Model contours are overlaid. The NO-PIPE version is displayed in panel (a), the LEAKY-PIPE version in panel (b), the PIPE in panel (c) and the SLOW in panel (d). The contour interval is 0.25 years.

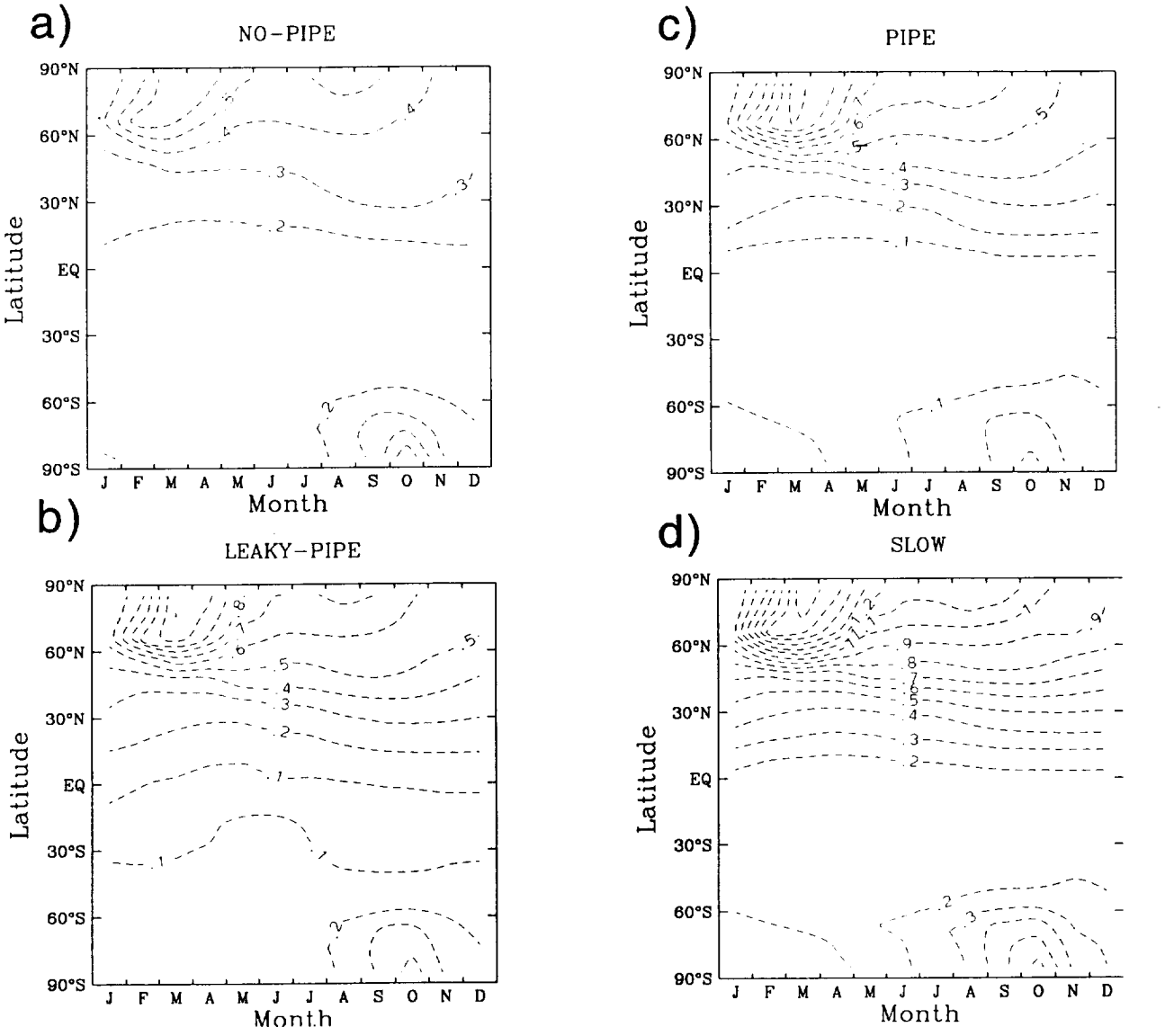

Figure 7: Calculated change in column ozone (%) due to an HSCT perturbation scenario of EI(NO_x)=5 with 500 aircraft for a 2015 atmosphere with background aerosols. The NO-PIPE version is displayed in panel (a), the LEAKY-PIPE version in panel (b), the PIPE in panel (c) and the SLOW in panel (d). The contour interval is 0.1%.

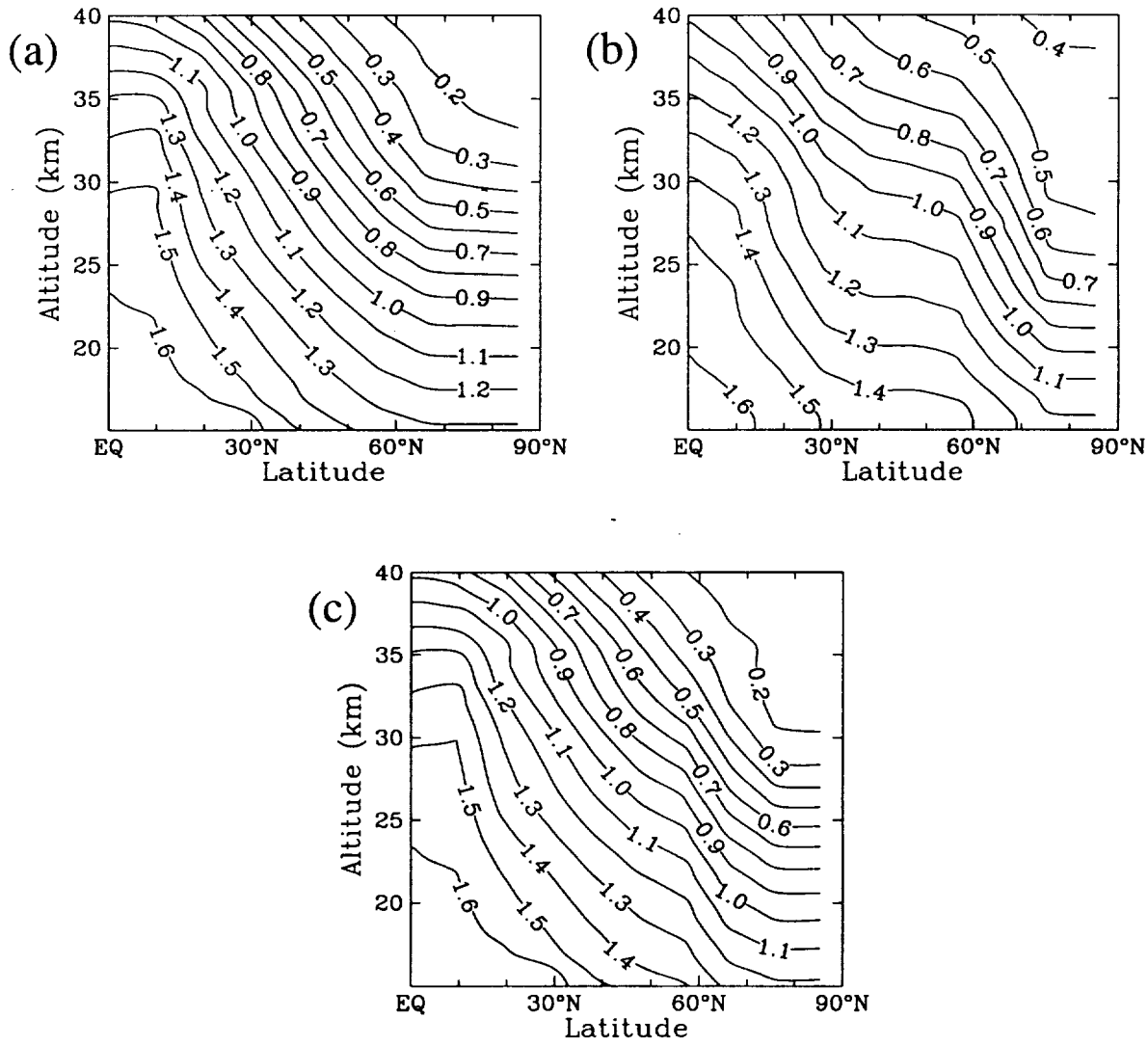

Figure 8: Latitude-altitude distribution of CH_4 mixing ratio (ppmv) in the northern hemisphere for February (a) as simulated by the AER 2-D CTM, (b) from UARS observations (Randel et al., 1998), and (c) as simulated by the AER 2-D CTM with polar barrier.

Appendix A

"A Comparison of Observations and Model Simulations of NO_x/NO_y in the Lower Stratosphere"

by R. S. Gao, D. W. Fahey, L. A. Del Negro, S. G. Donnelly, E. R. Keim, L. Teverovski, P. O. Wennberg, T. F. Hanisco, M. H. Proffitt, J. J. Margitan, J. C. Wilson, J. W. Elkins, R. M. Stimpfle, R. C. Cohen, C. T. McElroy, T. P. Bui, R. J. Salawitch, S. S. Brown, A. R. Ravishankara, R. W. Portmann, M. K. W. Ko, D. K. Weisenstein, and P. A. Newman

Submitted to Geophysical Research Letters

NAS5-97039: Semiannual Report on
Coupling Processes between Atmospheric Chemistry and Climate

A comparison of observations and model simulations of NO_x/NO_y in the lower stratosphere

R. S. Gao,[1,2] D. W. Fahey[1,2], L. A. Del Negro[1,2,3], S. G. Donnelly[1,2], E. R. Keim[4], J. A. Neuman[1,2], E. Teverovski[1,2], P. O. Wennberg[5], T. F. Hanisco[6], E. J. Lanzendorf[6], M. H. Proffitt[1,2], J. J. Margitan[7], J. C. Wilson[8], J. W. Elkins[9], R. M. Stimpfle[6], R. C. Cohen[10], C. T. McElroy[11], T. P. Bui[12], R. J. Salawitch[7], S. S. Brown[1,2], A. R. Ravishankara[1,2,3], R. W. Portmann[1], M. K. W. Ko[13], D. K. Weisenstein[13], and P. A. Newman[14]

Abstract. Extensive airborne measurements of the reactive nitrogen reservoir (NO_y) and its component nitric oxide (NO) have been made in the lower stratosphere. Box model simulations that are constrained by observations of radical and long-lived species and which include heterogeneous chemistry systematically underpredict the NO_x (= NO + NO_2) to NO_y ratio. The model agreement is substantially improved if newly measured rate coefficients for the OH + HNO_3 and OH + NO_2 reactions are used. When included in 2-D models, the new rate coefficients significantly increase the calculated ozone loss due to NO_x and modestly change the calculated ozone abundances in the lower stratosphere. Ozone changes associated with the emissions of a fleet of supersonic aircraft are also altered.

Introduction

Understanding the mechanisms controlling the abundance of NO_y and its partitioning into component species is an essential requirement for understanding the stratospheric ozone (O_3) layer. Reactions involving NO_x form a catalytic O_3 destruction cycle and also moderate O_3 loss due to other cycles involving reactive hydrogen (HO_x) and halogens (ClO_x-BrO_x) [*cf. Wennberg et al.*, 1994]. The partitioning of the NO_y reservoir between NO_x and other component species involves gas-phase and heterogeneous reactions as well as photolytic processes (see Figure 1) [*cf. Gao et al.*, 1997]. We present here extensive new measurements of NO and NO_y obtained in the high latitude lower stratosphere during summer. This data set provides a unique opportunity to test our understanding of the gas-phase chemistry linking NO_x and nitric acid (HNO_3), which is generally the most abundant NO_y species. Because the continuous daylight present at summer high latitudes limits the heterogeneous production of HNO_3 by N_2O_5 hydrolysis, gas-phase reactions primarily control the balance between NO_x and NO_y. Outside summer polar regions, the N_2O_5 hydrolysis reaction occurring on stratospheric sulfate aerosols is a more important sink of NO_x [*cf. Fahey et al.*, 1993], particularly in the lower stratosphere during winter when heterogeneous pathways account for most of the HNO_3 production [*cf. Gao et al.*, 1997].

Observations and box model description

The observational data set used here was acquired with instruments on board the NASA ER-2 high altitude aircraft during the Photochemistry of Ozone Loss in the Arctic Region In Summer (POLARIS) mission. The mission used deployment sites at latitudes of 37°N, 65°N, and 24°N. In the present study, data from 23 flights are used to examine NO_x/NO_y at high latitudes (> 60°N) in late spring, summer, and early fall periods, and in the tropics in early fall.

Measurements of NO and NO_y are made with a three-channel chemiluminescence detector [*Gao et al.*, 1997]. Because NO_2 measurements are not available for all flights, NO_2 values inferred from the steady state relationship (NO_2^*) [*Gao et al.*, 1997] are used throughout for consistency. The agreement between average NO_2^* and observed NO_2 values during POLARIS is within 10% (*L. A. Del Negro et al.*, Comparison of modeled and observed values of NO_2 and J_{NO_2} during the POLARIS mission, submitted to *J. Geophys. Res.*, 1998). The uncertainty of the NO_x/NO_y measurements is estimated to be ±20%. Measured aerosol surface area (SA) densities varied between 0.5 and 1.5 $\mu m^2 cm^{-3}$ in the data set used here.

A photochemical steady state box model that includes only the processes shown in Figure 1 is used to predict NO_x/NO_y in a sampled air parcel. The reaction set used in the model is a subset of the more comprehensive set used by *Salawitch et al.* [1994]. The model is constrained by observed values of NO, OH, ClO, O_3, SA, pressure and temperature, and column O_3 above the aircraft [see references in *Gao et al.*, 1997 for instrument details]. Because NO, OH, and ClO concentrations approach zero at high solar zenith angles (SZAs), data gathered at SZA > 85° are not used in this work. The diurnal dependence of the OH radical was determined empirically and normalized here to values observed along the flight track [*Wennberg et al.*, 1994; *T. F. Hanisco et al.*, unpublished data, 1999]. Modeled $ClONO_2$ values agree with POLARIS in situ observations to within 20% (*R. M. Stimpfle et al.*, The coupling of $ClONO_2$, ClO, and NO_2 in the lower stratosphere from in-situ observations using the NASA ER-2 aircraft, submitted to *J. Geophys. Res.*, 1998). Model BrO values are estimated by calculating the steady state partitioning of the Br_y reservoir as estimated from organic bromine observations [*Wamsley et al.*, 1998]. Unless otherwise noted, gas-phase rate coefficients, absorption cross sections, and reactive uptake coefficients on aerosol are taken from NASA JPL-97 recommendations [*DeMore et al.*, 1997]. Photolysis rates are calculated using a radiation scattering model [*Salawitch et al.*, 1994] which includes effects of overhead O_3, albedo and cloud heights. Reactive uptake coefficients of 0.1 and 0.8 are used for N_2O_5 and $BrONO_2$, respectively. The model does not include $ClONO_2$ hydrolysis since the reactive lifetime in sampled air parcels exceeds 100 days and thus this process has a negligible effect on NO_x/NO_y [*Robinson et al.*, 1997]. With input parameters averaged or interpolated to 100 s intervals, the model is run to a diurnal steady state to yield a value of NO_y consistent with measured NO and rate parameters used in the model. The NO_x/NO_y deduced in this way is then compared with that inferred from NO_2^* and the measured values of NO and NO_y.

Results

The comparison of observed and modeled NO_x/NO_y shown in Figure 2A, includes all stratospheric data from altitudes between 17 and 20 km (50 mb < pressure < 80 mb) with temperatures greater than 204K. The approximately 200,000 s of data are distributed in latitude between 0° and 90°N (< 40°: 5%; 40° - 60°: 17%; > 60°: 78%). In high latitude summer, NO_x reaches 3 parts per billion by volume (ppbv) with NO_x/NO_y in the range of 0.2 to 0.3. Although similar NO_x/NO_y ratios can also be found in the tropical lower stratosphere, the associated NO_x values are typically much less than 3 ppbv.

Most of the steady state model values of NO_x/NO_y fall significantly below observed values. The linear fit (forced through the origin) to the model/data regression has a slope of 0.65. The regression remains virtually unchanged if J_{NO_2} is altered to account for the small difference between NO_2^* and observed NO_2 values because J_{NO_2} changes affect NO_2 values on both axes in Figure 2A.

The diurnal steady state assumption is unlikely to be the cause of the observation-model discrepancy in Figure 2A. Back trajectories of the sampled air parcels were calculated using National Center for Environmental Prediction (NCEP) analyzed winds and temperatures. For each parcel, the accumulated latitude change over the previous 10 days was calculated using a weighting function inversely related to the time before aircraft sampling. When those parcels with an effective latitude change of 5° or more (~ 70% of the data) are excluded from the data set, the regression fit to the remaining data is not significantly changed.

The model parameterization of N_2O_5 hydrolysis is also unlikely to be the cause of the NO_x/NO_y discrepancy. Using NCEP back trajectories, sampled air parcels that had recently experienced nearly continuous solar illumination were identified. The acceptance criterion was an SZA of less than 93° for 90% of the preceding 5 day period. As solar illumination becomes continuous, the diurnal conversion of NO_x to HNO_3 through N_2O_5 formation and hydrolysis becomes negligible [*Farman et al.*, 1985; *Brühl et al.*, 1998] and hence the contribution of N_2O_5 hydrolysis to NO_x/NO_y also becomes negligible. The separately averaged data sets in Figure 2A, show that, overall, these selected data points are nearly indistinguishable as a group from those that experience interrupted solar illumination. In contrast to the diminished role of N_2O_5 hydrolysis, the contribution of $BrONO_2$ hydrolysis to reducing NO_x/NO_y is greatest for the continuously illuminated parcels [*Randeniya et al.*, 1997]. However, $BrONO_2$ hydrolysis reduces NO_x/NO_y by a maximum of only 5 - 10%. Thus, the hydrolysis reactions of N_2O_5, $ClONO_2$, and $BrONO_2$ are not effective enough individually or collectively to cause the systematic discrepancy shown in Figure 2A.

In air parcels in which the heterogeneous hydrolysis reactions in Figure 1 do not play a strong role, NO_x/NO_y is primarily controlled by the gas-phase reactions:

$$OH + NO_2 + M \rightarrow HNO_3 + M \quad (1)$$

$$OH + HNO_3 \rightarrow NO_3 + H_2O \quad (2)$$

$$HNO_3 + h\nu \rightarrow OH + NO_2 \quad (3)$$

where M is O_2 or N_2. Only a few measurements of the rate coefficient for (1) and (2) (k_1 and k_2) are available at lower stratospheric temperatures (220 ± 20K) and pressures (50 - 150 mb) [*DeMore et al.*, 1997]. *Donahue et al.* [1997] first suggested that JPL-97 values for k_1 may be too high for stratospheric conditions. Recently, *Dransfield et al.* [1999] and *Brown et al.* [1999] reported laboratory measurements of k_1 for stratospheric conditions that are about 20 - 30% lower than JPL-97 values but consistent with the few previous measurements available below 298K. *Brown et al.* [1999] also show that k_2 in the lower stratosphere is higher (up to 50%) than JPL-97 values.

Incorporating the new values of k_1 and k_2 of *Brown et al.* [1999] in the model significantly improves the overall agreement with the observations (Figure 2B). The linear fit (forced through the origin) with the new model results has a slope of 0.90. In a similar analysis using balloon observations of NO_x/NO_y at ER-2 altitudes and above, agreement to within 10% is achieved for a 35% reduction of k_1 from JPL-97 values [*Osterman et al.*, 1999]. The *Brown et al.* values of k_1 are not expected to substantially affect the *Gao et al.* [1997] results for winter polar NO_y partitioning since N_2O_5 hydrolysis is generally faster than reaction (1) under the conditions sampled. In contrast, an increase in k_2 will lead to a calculated increase in NO_x/NO_y during winter.

An increase of the HNO_3 photolysis rate in (3) would also improve the observation-model comparisons in Figure 2. In the absence of changes to k_1 and k_2, an increase of approxi-

mately 70% is required to yield a regression slope of 0,9. Such a large increase exceeds the reported uncertainties in the underlying measurements of the temperature dependent HNO_3 absorption cross section for lower stratospheric conditions [*Burkholder et al.*, 1993] or in the uncertainties associated with the radiation field calculations [*Gao et al.*, 1997; *Salawitch et al.*, 1994].

Implications

The 2-D dynamical-chemical-radiative model of *Garcia and Solomon* (GS) [1994] and the AER chemistry-transport model [*Weisenstein et al.*, 1996] were used to examine the effects of the *Brown et al.* rates on O_3 and the principal ozone catalytic loss cycles at high latitudes in summer. The results shown in Figure 3 include altitudes between 15 and 40 km in the stratospheric ozone layer in July at 59°N to illustrate the effect of the new k_1 and k_2 values over a range of model temperatures and other conditions. The important features in Figure 3 are (i) that large changes in the rates that control NO_x/NO_y yield much smaller changes in the ozone distribution in the lower stratosphere due to the corresponding changes in HO_x, ClO_x, and BrO_x abundances, and (ii) that the new rates result in a 'cross-over' near 20 km from an increased to a decreased value of the total O_3 destruction rate. Throughout most of the 15 - 40 km region, the magnitude of the NO_x-catalyzed destruction increases (up to 10% near 25 km when expressed as a percentage of the new total O_3 destruction rate) as a direct result of higher NO_x/NO_y values while the contributions from the BrO_x-ClO_x and HO_x catalytic cycles decrease because of moderation by NO_x. Above 25 km, NO_x/NO_y approaches unity and the sensitivity of the O_3 loss cycles to the rate coefficient changes approaches zero. At 25 km, the net increase in O_3 destruction rates reaches a maximum. Because changes in k_2 are largest at low temperatures and affect the abundances of both NO_x and HO_x, the sensitivity of the BrO_x-ClO_x and HO_x cycles to increases in NO_x/NO_x is largest below 25 km and results in a net decrease in the total O_3 loss rate. Changes in the vertical distribution of O_3 due to the new rates are small (< 5%) throughout the 15 - 40 km region, consistent with the calculated changes in the O_3 loss rate. *Brown et al.* [1999] show that lower-latitude O_3 changes are also small (< 2%) in the GS model using the new k_1 and k_2 values and an increased value for the $O + NO_2$ rate coefficient.

The increased contribution of the NO_x cycle to O_3 loss rates at mid and high latitudes modifies how emissions from a proposed High Speed Civil Transport (HSCT) stratospheric aircraft fleet are expected to change O_3 in the lower stratosphere [*Stolarski et al.*, 1995]. Whether the *Brown et al.* rates will lead to a larger or smaller depletion for a particular HSCT scenario depends sensitively on the relative emissions of NO_x and sulfur from an HSCT engine. The sulfur emission index (EI) and exhaust plume processes determine the SA changes of the background sulfate aerosol. As an example, Table 1 shows how the *Brown et al.* k_1 and k_2 values affect O_3 column amounts at 59°N in summer for two key HSCT fleet scenarios in a 2015 and 2050 atmosphere. With no sulfur emissions, the changes in the rate coefficients of k_1 and k_2 result in slightly larger O_3 depletion because the role of NO_x in catalytic O_3 loss is greater than its role in moderating the HO_x and halogen cycles. When sulfur is also emitted, the formation of sulfate particles in the plume and their accumulation in the atmosphere causes an increase in background SA densities. Larger SA densities reduce NO_x values through N_2O_5 hydrolysis (for both the NO_x emitted by the aircraft and NO_x in the background atmosphere), resulting in a decrease in the O_3 removal by the NO_x loss cycle compared to the atmosphere without aircraft. The NO_x reduction due to increased SA densities in the atmosphere increases

the HO_x and active halogen concentrations, resulting in increases for the corresponding O_3 removal cycles. The effects of increased NO_x concentrations due to aircraft emission must be considered in conjunction with the effects of increased SA densities. The use of the *Brown et al.* rates in this case results in less O_3 depletion because more effective moderation of the HO_x and halogen loss cycles by aircraft-emitted NO_x partially mitigates the effect of aerosol changes.

Concluding remarks

The in situ aircraft observations presented here represent a large new data set with which to examine stratospheric NO_x/NO_y over a wide range of latitude and season in the lower stratosphere. Representative box model calculations systematically underpredict the observed ratio by about 40%. Because the discrepancy remains in air parcels with continuos solar exposure, the parameterization of the N_2O_5 hydrolysis reaction is unlikely to be the cause. The use of recent laboratory results for the OH + NO_2 and OH + HNO_3 reaction rate coefficients from *Brown et al.* [1999] significantly improves the comparison of measured and modeled NO_x/NO_y for most sampled air parcels. The effect of the rate changes and associated NO_x increases on O_3 concentrations calculated in 2-D models is small (< 5%) throughout most of the lower stratosphere because of the interdependence of the NO_x, BrO_x-ClO_x, and HO_x catalytic loss cycles.

Acknowledgments. We thank the pilots and ground crew of the NASA ER-2 aircraft. This work is supported by the NASA Upper Atmospheric Research Program and the Atmospheric Effects of Aviation Project.

References

Brown, S. S., T. Gierczak, R. W. Portmann, R. K. Talukdar, J. B. Burkholder, and A. R. Ravishankara, Role of nitrogen oxides in the lower stratosphere: A reevaluation based on laboratory studies, *Geophys. Res. Lett.*, this issue, 1999.

Brühl, C., P. J. Crutzen, and J.-U. Grooß, High-latitude, summertime NO_x activation and seasonal ozone decline in the lower stratosphere: Model calculations based on observations by HALOE on UARS, *J. Geophys. Res., 103*, 3587-3597, 1998.

Burkholder, J. B., R. K. Talukdar, A. R. Ravishankara, and S. Solomon, Temperature dependence of the HNO_3 UV absorption cross sections, *J. Geophys. Res., 98*, 22937-22948, 1993.

DeMore. W. B., et al., Chemical kinetics and photochemical data for use in stratospheric modeling, *JPL Publ. 97-4*, Jet Propul. Lab., Pasadena, Calif., 1997.

Donahue, N. M., M. Dubey, R. Mohrschladt, K. L. Demerjian, and J. G. Anderson, A high pressure flow study of the reactions OH + NO_x → $HONO_x$: Errors in the falloff region, *J. Geophys. Res., 102*, 6159-6168, 1997.

Dransfield, T. J., K. K. Perkins, N. M. Donahue, J. G. Anderson, M. M. Sprengnether, and K. L. Demerjian, Temperature and pressure dependent kinetics of the gas-phase reaction of the hydroxyl radical with nitrogen dioxide, *Geophys. Res. Lett.*, in press, 1999.

Fahey, D. W., *et al.*, In situ measurements constraining the role of sulphate aerosols in mid-latitude ozone depletion, *Science, 363*, 509-514, 1993.

Farman, J. C., R. J. Murgatroyd, A. M. Silnickas, and B. A. Thrush, Ozone photochemistry in the Antarctic stratosphere in summer, *Q. J. Royal Met. Soc., 111*, 1013-1028, 1985.

Garcia, R. R. and S. Solomon, A new numerical model of the middle atmosphere: 2. Ozone and related species, *J. Geophys. Res., 99*, 12937-12951, 1994.

Gao, R. S., et al., Partitioning of the reactive nitrogen reservoir in the lower stratosphere of the southern hemisphere: Observations and modeling, *J. Geophys. Res., 102*, 3935-3949, 1997.

Osterman, G. B., B. Sen, G. C. Toon, R. J. Salawitch, J. J. Margitan, J.-F. Blavier, D. W. Fahey, and R. S. Gao, The budget and partitioning of

reactive nitrogen species in the Arctic stratosphere, *Geophys. Res. Lett.*, this issue, 1999

Randeniya, L. K., P. F. Vohralik, I. C. Plumb, and K. R. Ryan, Heterogeneous $BrONO_2$ hydrolysis: Effect on NO_2 columns and ozone at high latitude in summer, *J. Geophys. Res.*, *102*, 23,543-23,557, 1997.

Robinson, G. N., D. R. Worsnop, J. T. Jayne, C. E. Kolb, and P. Davidovits, Heterogeneous uptake of $ClONO_2$ and N_2O_5 by sulfuric acid solutions, *J. Geophys. Res.*, *102*, 3583-3601, 1997.

Salawitch, R. J., et al., The diurnal variation of hydrogen, nitrogen, and chlorine radicals: Implications for the heterogeneous production of HNO_2, *Geophys. Res. Lett.*, *21*, 2551-2554, 1994.

Stolarski, R. S., et al., 1995 Scientific assessment of the atmospheric effects of stratospheric aircraft, *NASA Ref. Publ. 1381*, Washington, D.C., 1995.

Wamsley, P. R. et al., Distribution of halon-1211 in the upper troposphere and lower stratosphere and the 1994 total bromine budget, *J. Geophys. Res.*, *103*, 1513-1526, 1998.

Weisenstein, D. K., et al., Potential impact of SO_2 emissions from stratospheric aircraft on ozone, *Geophys. Res. Lett.*, *23*, 161-164, 1996.

Wennberg, P. O., et al., Removal of stratospheric O_3 by radicals: In situ measurements of OH, HO_2, NO_2, ClO, and BrO, *Science*, *266*, 398-404, 1994.

S. S. Brown, S. G. Donnelly, D. W. Fahey, R. S. Gao, J. A. Neuman, R. W. Portmann, M. J. Proffitt, and E. Teverovski, NOAA Aeronomy Laboratory, Boulder, Colorado, and Cooperative Institute for Research in Environmental Sciences (CIRES), University of Colorado, Boulder, CO.

T. P. Bui, NASA Ames Research Center, Moffett Field, CA.

R. C. Cohen, Department of Chemistry, University of California, Berkeley, CA.

L. A. Del Negro, A. R. Ravishankara, NOAA Aeronomy Laboratory, Boulder, CO; CIRES; Department of Chemistry and Biochemistry, University of Colorado, Boulder, CO.

J. W. Elkins, NOAA Climate Monitoring and Diagnostics Laboratory, Boulder, CO.

T. F. Hanisco, E. J. Lanzendorf, R. M. Stimpfle, Department of Chemistry, Harvard University, Cambridge, MA.

E. R. Keim, The Aerospace Corporation, Los Angeles, CA

M. K. W. Ko, D. K. Weisenstein, Atmospheric Environment Research, Inc., Cambridge, MA.

J. J. Margitan, R. J. Salawitch, NASA Jet Propulsion Laboratory, Pasadena, CA.

C. T. McElroy, Atmospheric Environment Service, Downsview, Ontario, Canada.

P. A. Newman, NASA Goddard Space Flight Center, Greenbelt, MD.

P. O. Wennberg, California Institute of Technology, Pasadena, CA

J. C. Wilson, Department of Engineering, University of Denver, Denver, CO

(Received November 24, 1998; revised February 17, 1999; accepted February 22, 1999.)

---

[1]Aeronomy Laboratory, National Oceanic and Atmospheric Administration, Boulder, CO

[2]Cooperative Institute for Research in Environmental Sciences, University of Colorado, Boulder, CO

[3]Department of Chemistry and Biochemistry, University of Colorado, Boulder, CO

[4]The Aerospace Corporation, Los Angeles, CA

[5]Division of Geology and Planetary Sciences, California Institute of Technology, Pasadena, CA

[6]Department of Chemistry, Harvard University, Cambridge, MA

[7]Jet Propulsion Laboratory, California Institute of Technology, Pasadena, CA

[8]Department of Engineering, University of Denver, Denver, CO

[9]Climate Monitoring and Diagnostics Laboratory, National Oceanic and Atmospheric Administration, Boulder, CO

[10]Department of Chemistry, University of California, Berkeley, CA

[11]Atmospheric Environment Service, Downsview, Ontario, Canada

[12]NASA Ames Research Center, Moffett Field, CA

[13]Atmospheric Environment Research, Inc., Cambridge, MA

[14]NASA Goddard Space Flight Center, Greenbelt, MD

Table 1. Column O_3 change (%) at 59°N in July[a]

EI(SO_2) (g/kg fuel)	JPL 97 rates	*Brown et al.* rates for (1) and (2)
0	-0.5/-0.4	-0.6/-0.6
0.4[b]	-1.3/-0.9	-1.0/-0.5

[a] AER model results for the scenario of 500 HSCT aircraft operating at Mach 2.4 near 18 km cruise altitude with an emission index (EI) of (NO_x) of 5 g/kg fuel. Values are noted for both 2015 and 2050 models years as '2015/2050'. Similar values are calculated for average hemispheric O_3 column changes.

[b] With 50% conversion to small sulfate particles in the plume.

Figure 1. Schematic of the reaction pathways between the principal NO_y component species in the lower stratosphere. Photolysis reactions are indicated by hv. 'Sulfate aerosol' denotes heterogeneous reactions on background aerosol particles.

Figure 2. Comparison of modeled and measured values of NO_x/NO_y from POLARIS. The symbols are averages of data as grouped by increasing NO_x/NO_y value. Open symbols are averages of 80 points, each of which represented 100 s of observational data. The solid symbols are separate averages (84 points of 100 s data) for those POLARIS observations for which the sampled air parcel experienced near-continuous solar illumination for the preceding 5 days. The horizontal and vertical bars on each symbol represent the 1-σ sample standard deviation within each group of measured and modeled values, respectively. Results are shown using the model with JPL recommended rate coefficient values (panel A) and with the *Brown et al.* [1999] rate coefficient expressions for (1) and (2) (panel B). The solid and dashed lines represent the 1:1 and 1:2 regression slopes, respectively.

Figure 3. GS model results vs altitude for percentage changes in ozone, its total destruction rate, and the contributions of the NO_x, HO_x, and halogen catalytic cycles for average July 1990 conditions at 59°N with background aerosol conditions. The changes are those that result from using the new *Brown et al.* [1999] values for k_1 and k_2. The percentage changes of the catalytic cycles are shown with respect to the new total ozone loss rate. The percentage changes between the new and old values of the individual loss cycles are larger. For example, at 20 km the NO_x, HO_x, and halogen cycle changes are +23%, -10%, and -22%, respectively. Nearly identical results are obtained with the AER model. The representativeness of the GS model was checked by comparing the average observations at 65°N with the nearest model grid point (64°N). Noon model values of NO_x/NO_y are somewhat lower (< 25%) in the 15 - 20 km region at high latitudes. The longer-lived NO_y, Cl_y, and O_3 species are within 10 - 20% of the average observed values between 15 and 20 km.

Figure 1. Schematic of the reaction pathways between the principal NO_y component species in the lower stratosphere. Photolysis reactions are indicated by hv. 'Sulfate aerosol' denotes heterogeneous reactions on background aerosol particles.

Figure 2. Comparison of modeled and measured values of NO_x/NO_y from POLARIS. The symbols are averages of data as grouped by increasing NO_x/NO_y value. Open symbols are averages of 80 points, each of which represented 100 s of observational data. The solid symbols are separate averages (84 points of 100 s data) for those POLARIS observations for which the sampled air parcel experienced near-continuous solar illumination for the preceding 5 days. The horizontal and vertical bars on each symbol represent the 1-σ sample standard deviation within each group of measured and modeled values, respectively. Results are shown using the model with JPL recommended rate coefficient values (panel A) and with the *Brown et al.* [1999] rate coefficient expressions for (1) and (2) (panel B). The solid and dashed lines represent the 1:1 and 1:2 regression slopes, respectively.

Figure 3. GS model results vs altitude for percentage changes in ozone, its total destruction rate, and the contributions of the NO_x, HO_x, and halogen catalytic cycles for average July 1990 conditions at 59°N with background aerosol conditions. The changes are those that result from using the new *Brown et al.* [1999] values for k_1 and k_2. The percentage changes of the catalytic cycles are shown with respect to the new total ozone loss rate. The percentage changes between the new and old values of the individual loss cycles are larger. For example, at 20 km the NO_x, HO_x, and halogen cycle changes are +23%, -10%, and -22%, respectively. Nearly identical results are obtained with the AER model. The representativeness of the GS model was checked by comparing the average observations at 65°N with the nearest model grid point (64°N). Noon model values of NO_x/NO_y are somewhat lower (< 25%) in the 15 - 20 km region at high latitudes. The longer-lived NO_y, Cl_y, and O_3 species are within 10 - 20% of the average observed values between 15 and 20 km.

GAO ET AL.: NO_x/NO_y IN THE LOWER STRATOSPHERE

GAO ET AL.: NO_x/NO_y IN THE LOWER STRATOSPHERE

Top.....top.....top.....top.....top.....top.....top.....top.....top

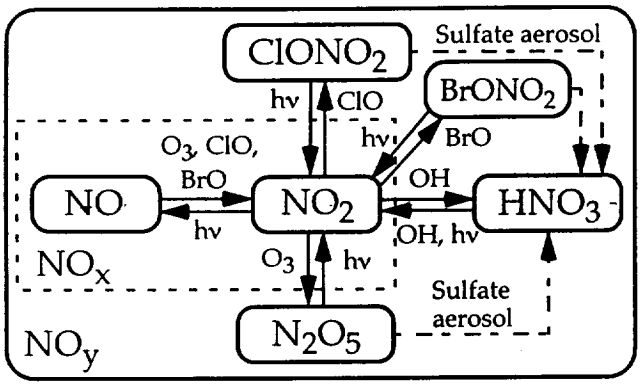

Figure 1, Gao et al., MS #4330

Top.....top.....top.....top.....top.....top.....top.....top.....top

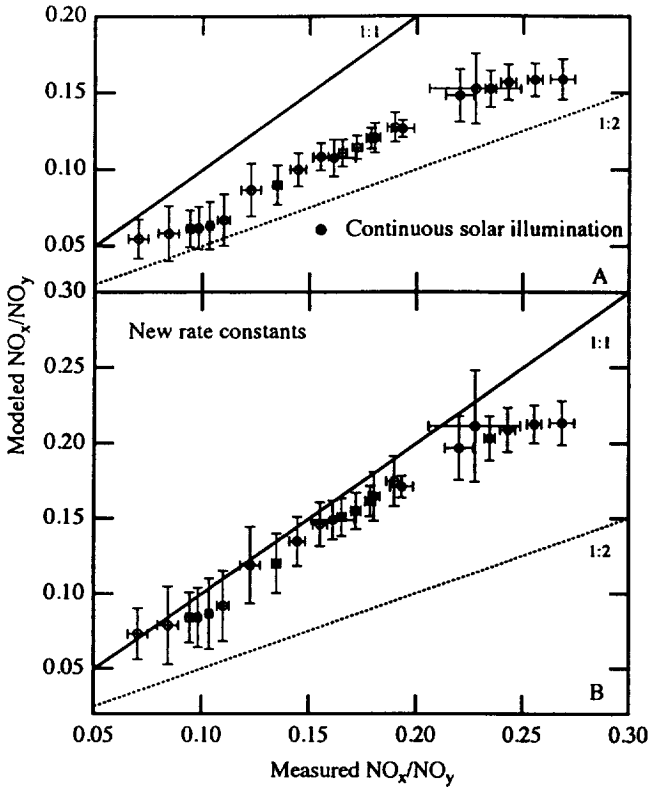

Figure 2, Gao et al., MS #4330.

Top.....top.....top.....top.....top.....top.....top.....top.....top

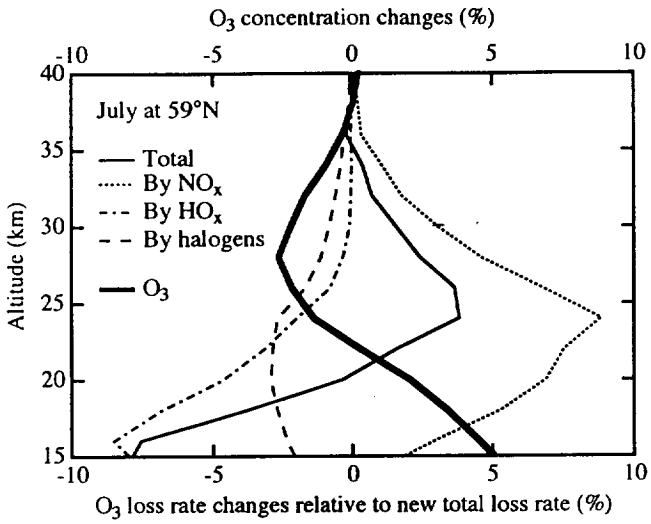

Figure 3, Gao et al., MS #4330

Appendix B

"The Simulation of the Polar Barriers in a 2-D CTM
by Adjusting the Eddy Diffusion Coefficients using UARS CH_4 Data"
by R.-L. Shia, W. J. Randel, M. K. W. Ko, J. Rodriguez, and C. Scott

Presented at
1998 Fall Meeting of the
Americal Geophysical Union,
San Francisco, CA

NAS5-97039: Semiannual Report on
Coupling Processes between Atmospheric Chemistry and Climate